IEEE Access
Multidisciplinary | Rapid Review | Open Access Journal

Received December 7, 2017, accepted January 22, 2018, date of publication February 8, 2018, date of current version March 13, 2018.

Digital Object Identifier 10.1109/ACCESS.2018.2803791

Detection and Correction of Element Failures Using a Cumulative Sum Scheme for Active Phased Arrays

YEN-SHENG CHEN, (Member, IEEE), AND I-LIN TSAI
Department of Electronic Engineering, National Taipei University of Technology, Taipei 10608, Taiwan (e-mail: yschen@ntut.edu.tw)

Corresponding author: Yen-Sheng Chen (yschen@ntut.edu.tw)

This work was supported in part by the National Chung-Shan Institute of Science and Technology, Taiwan, under Contract XU05122P-CS and in part by the Ministry of Science and Technology, Taiwan, under Contract MOST 107-2636-E-027-001.

ABSTRACT In this paper, we propose a novel technique that integrates the detection of element failures and the correction of damaged patterns into a systematic process for active phased arrays. The proposed technique uses the framework of mutual coupling method, and its kernel is based on a cumulative sum (CUSUM) scheme that monitors attenuators and phase shifters inside transmit/receive modules. The proposed method is organized into two phases. The phase one copes with the detection of failed components. By cumulating time-series data, the CUSUM can readily detect the defective elements even though very small shifts are examined. We test the effectiveness through a 448-element active phased array. The measured results show that no type I error is found, and the type II error of the most challenging scenario is significantly reduced. The phase two aims at the correction of patterns. By integrating the experimental result provided by the phase one and a least-squares method, the proposed technique can determine the new excitations leading to reduced sidelobe levels and a desired main beam characteristic. The capability is verified through three examples including linear and planar arrays. The results show that the proposed method can correct the damaged patterns with low computational complexity.

INDEX TERMS Antenna arrays, attenuators, failure analysis, fault detection, phase shifters, phased arrays, planar arrays.

I. INTRODUCTION

Active phased array technology has been deployed in various electronic applications where high directivity and/or electronic beam scanning is desired. In active phased array systems, each antenna element is driven by a dedicated transmit/receive (TR) module, which incorporates amplification with phase shift into that antenna element, as shown in Fig. 1. When a beam steering computer synthesizes a desired radiation pattern, these TR modules follow a perfect hardware assumption where the components can be controlled accurately; however, when deploying a very large number of TR modules after long periods of continuous operation, practical active phased array systems may suffer from hardware impairment [1]–[3]. Given this large number of elements presented in an array, there is a possibility that one or more components are failed [4]. Such failed amplifiers or phase shifters degrade radiation patterns. Thus, detecting the failure of TR modules and further correcting the pattern is important.

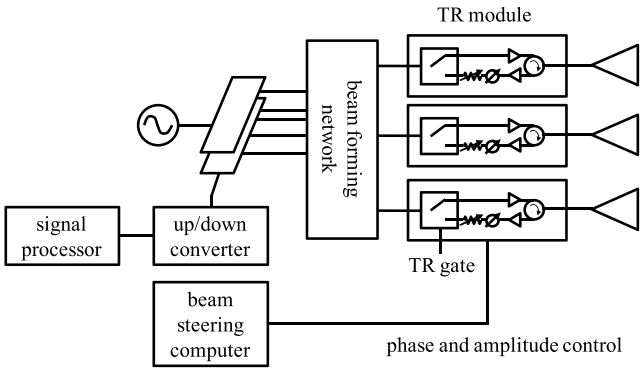

FIGURE 1. Block diagram of an active phased array.

The method of detecting element failures can be categorized into on-ground calibration and on-board calibration, which follow the definition from the test of space radio instruments. The on-ground calibration means that finding out the positions of faulty elements in an array before the

array is launched for its operational environment, such as a battlefield or space platform. This method requires a far-field test environment or an anechoic chamber, and it needs an algorithm to detect the number and the locations of faulty elements by comparing the distorted far-field or near-field pattern with the failed elements included to the original ''fault-free'' one. Toward this end, the algorithms for data comparison include genetic algorithms [5]–[9], neural networks [10]–[13], compressive sensing [14]–[17], back-propagation method [18], matrix method [19], the theory of random partial Fourier matrices [20], the assessment of peak sidelobe level (SLL) [21], multiple signal classification algorithm [22], and bacteria foraging optimization [23]. However, the use of iterative optimization algorithms is time-consuming, and this approach cannot real-time monitor the presence of faulty elements and further perform on-line calibration.

In contrast, the on-board calibration can be applied to deployed active phased arrays in a self-calibrating manner. This method implements a measurement system that integrates an antenna measurement facility and a detection algorithm along with the active phased array, detecting element failures via evaluating over-the-air (OTA) data collected by the test port. Earlier studies implement the on-board calibration by using mutual coupling method [24]–[35], rotating-element electric-field vector method [35]–[38], near-field scanning method via peripheral fixed probes [39]–[42], calibration lines [43], [44], phase-shift measurement method [45], [46], and phase-match method [47]. Among these techniques, the mutual coupling method adds internal calibrating circuits and uses mutual coupling to perform an automatic detection process on the array, without taking the array out of service [24]–[35]. This approach requires no external probe, thereby decreasing the weight, complexity, and cost to the system. Nevertheless, the mutual coupling method detects element failures by constructing specification limits, which reduce accuracy if the separation between a test antenna (TA) and an antenna under test (AUT) is large.

After the faulty elements have been identified, the correction of a damaged pattern is primarily concerned with the use of optimization algorithms. These algorithms nullify the failed elements, determining the new current excitations of the remaining elements that minimize the difference between the original pattern and the corrected pattern. Some optimization schemes have been reported, including genetic algorithms [48]–[52], simulating annealing [53], [54], particle swarm optimization [55], [56], vector space projection [57], differential search algorithm [58], cultural algorithm with differential evolution [59], firefly algorithm [60], bat algorithm [61], neural networks [62], conjugate gradient-based method [63], and linear/square approximations of array factor [64], [65]. Additionally, there are techniques that are not based on evolutionary computation. These methods develop an error minimization scheme using the introduction of pseudo-random fluctuations [66], signal replacement through a digitally beamforming array [67], active amplitude weighting using low sidelobe pattern synthesis [68], conjugate symmetry approach [69], almost difference sets [70], bias correction matrices [71], alternative projection algorithm [41], and a real-time case-based reasoning compensation technique [72]. However, those optimization-based algorithms are time-consuming due to blind-search features [48]–[65], which simply perform heuristic operators that improve solutions iteration-by-iteration. In addition, there is limited study that has integrated the detection of element failures and correction of damaged patterns into a systematic procedure. Most of the literature treats the pattern correction as a separate procedure from the fault finding [48]–[72]. The information on fault finding calculations does not transfer to the phase of pattern correction.

In this paper, we propose a novel technique that integrates the detection and correction of element failures into a systematic process for active phased arrays. This method is designed to monitor the attenuator and phase shifter inside TR modules. The framework is based on the mutual coupling method [24]–[35]. Our proposed method is developed from a statistical process control (SPC) method called cumulative sum (CUSUM) control charts, and its process is designed in two phases: the detection of faulty elements and the correction of damaged pattern. In the phase one, the CUSUM monitors two test statistics derived from S parameters. We will show that the conventional method [24]–[35] that uses specification limits increases a type I error if the spacing between the TA and the AUT is large, and this approach incurs a serious type II error as the smallest digital control code is tested. However, our proposed method overcomes these limitations. In the phase two, the new excitations for correcting the damaged pattern are calculated from the result of the phase one. The phase two exploits the measured data by using a least-squares method, requiring neither blind search nor iterative procedures [48]–[65]. The capability and efficiency of pattern correction will be demonstrated through linear arrays with Dolph-Chebyshev excitations and a planar array with a flat-top pattern.

II. HARDWARE ARCHITECTURE

Fig. 2 shows the active phased array to be demonstrated. It is a planar array that operates at S-band and is populated by 512 printed dipole elements arranged along a triangular placement by 32 rows and 16 columns. The 512 elements are divided into 16 subarrays that comprise 8×4 elements respectively. The spacing between the center of two horizontal and vertical elements are 0.99 and 0.49 free-space wavelengths of the low operational frequency, respectively. Although 512 elements are represented, the 2×8 elements located in each corner are disabled due to a power management concern; thus, there are 448 elements activated in this array. This active array is employed in a monopulse radar system that tracks the location of a target by comparing multiple simultaneous beams. The beam steering computer generates three simultaneous beams, including a sum beam

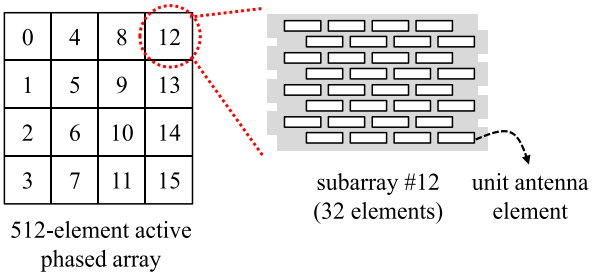

FIGURE 2. An active phased array that has 512 identical elements divided into 16 subarrays. 448 elements are activated.

and two difference beams, and the received signals correlated from the three beams can provide the angle estimate of a target.

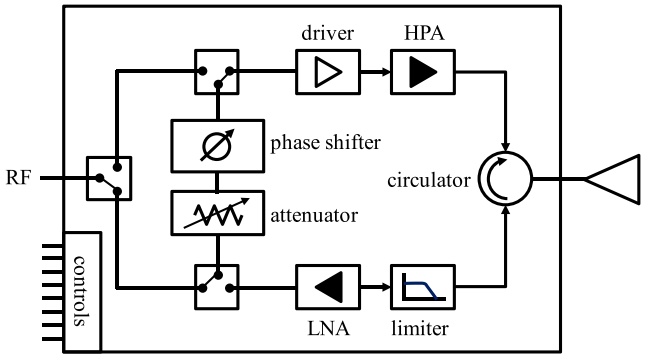

FIGURE 3. Block diagram of a TR module in an active phased array.

To generate the desired sum and difference beams, each antenna element is connected to a separate TR module, which consists of a variable attenuator, a variable phase shifter, a high power amplifier (HPA), a driver, a limiter, and a low noise amplifier (LNA). Fig. 3 shows the architecture of the TR module. This TR module employs the mode of alternate polarization in transmit and receive (ATAR), which can reduce the number of component used per channel and provide larger dynamic range in comparison with simultaneous transmit and simultaneous receive (STSR) mode and alternate polarization in transmit and simultaneous in reception (ATSR) [73]. Among the components depicted in Fig. 3, the variable attenuator and the variable phase shifter are the most crucial components for the beam forming purpose. The variability of the two components is implemented through a digitalization approach which employs a 6-bit 32 dB digital attenuator with an attenuation step of 0.5 dB and a 6-bit digital phase shifter that provides 360° phase coverage with a phase shift step of 5.625°. Table 1 shows the mapping of the control code to the resultant operation.

To detect the digital element failures for the attenuator and the phase shifter, we implement the framework of mutual coupling method [24]–[35]. Fig. 4 (a) represents the OTA test facility that comprises an AUT (denoted as port 1) along with an associated TR module and a TA (denoted as

TABLE 1. Digitalization method for TR modules.

Control code	Attenuator (dB)	Phase shifter (°)
000001	0.5	5.625
000010	1	11.25
000100	2	22.5
001000	4	45
010000	8	90
100000	16	180

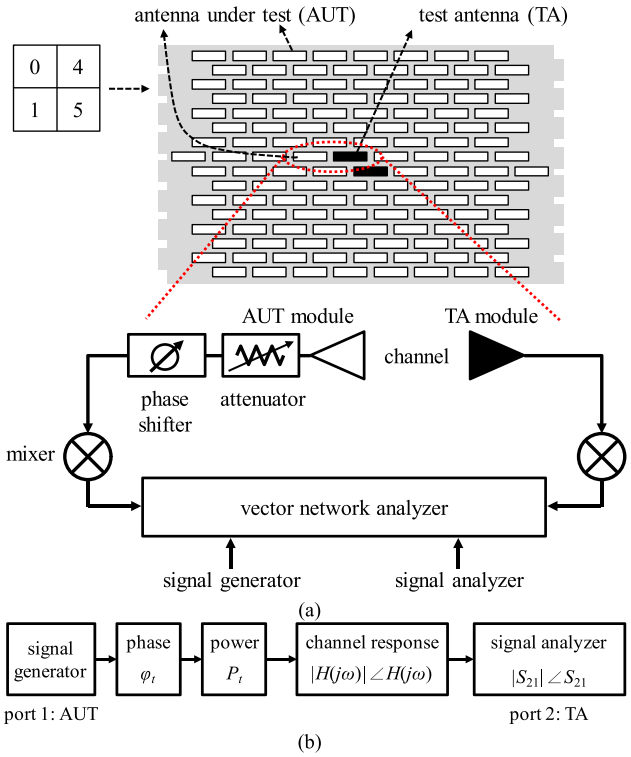

FIGURE 4. (a) Schematic of mutual coupling method for monitoring TR modules in an active phased array. (b) The *S* parameters used for detecting element failures.

port 2) module devoted to measure the mutual coupling between them. Besides the 448 elements that act as an AUT, this array inserts additional 8 TA modules. In particular, each dual TA modules serve a corner four subarrays as the test facility; one is operated for the detection purpose, and the other is intentionally made redundant. The TA module calibrates one AUT at a time, measuring the mutual coupling to monitor whether the attenuator/phase shifter of the AUT module is defective.

The detection loop is illustrated using Fig. 4 (b). The AUT module transmits a reference signal at first. This reference signal is added by an additional phase φ_t that results from the phase shifter, and its magnitude is multiplied by P_t caused by the attenuator. Such a transmitting signal is propagated by an OTA channel, the transfer function of which is denoted as $H(j\omega) = |H(j\omega)|\angle H(j\omega)$. Subsequently, the TA module measures the S_{21} as compared to the reference signal, expressed

as $|S_{21}| = |H(j\omega)| + P_t$ and $\angle S_{21} = \angle H(j\omega) + \varphi_t$. Thus, we can monitor the impairment of the attenuator and that of the phase shifter by evaluating $|S_{21}|$ and $\angle S_{21}$, respectively. However, the channel link between the AUT and the TA suffers from small- and large-scale fading due to various antenna positions and test distances, so the transfer function of a channel, namely $H(j\omega)$, has a stochastic nature. Accordingly, the two measured observations, including $|S_{21}|$ and $\angle S_{21}$, are also samples out of probability distribution functions, making the performance monitoring of the TR module a challenging stochastic problem.

III. PROPOSED TECHNIQUE

In spite of the stochastic nature of $|S_{21}|$ and $\angle S_{21}$, there have been numerous studies using deterministic schemes to determine whether impairment occurs. By such, the fading that results from the OTA channel is overlooked, and the probability of successful detection is reduced, as will be shown in Section IV.

In contrast, SPC takes the variation of $|S_{21}|$ and $\angle S_{21}$ due to the fading into account. SPC characterizes the fading as chance causes, detecting the assignable cause due to the element failure of a TR module. SPC takes advantage of a control chart, which is a graphical display of a measured test statistic versus time. The most widely-used SPC is Shewhart control charts [74], which develop an upper and a lower control limit by $T \pm 3\hat{\sigma}$, respectively, where T is a target value and $\hat{\sigma}$ is the standard deviation estimate of the test statistic. Shewhart charts show good performance in many practical situations; however, they are relatively insensitive to small shifts in the process. In our application, once the smallest control code of a TR module is defective, the accuracy of Shewhart control charts decreases dramatically.

To overcome the limitations of the conventional mutual coupling method and the Shewhart control chart, we propose a novel technique based on the CUSUM. As Shewhart control charts make use of only the information in the latest sample, they ignore a trend in the time-series data. In contrast, the CUSUM charts define the test statistic as the sum of the deviations of the incoming data from a target value. By combining information from multiple incoming samples, a small difference is thus converted into a significant one.

A. PHASE ONE: DETECTION OF FAULTY TR MODULES

Fig. 5 demonstrates the proposed technique that is cast into the phase of detection and the phase of correction. To begin with, the proposed technique collects the training dataset of $|S_{21}|$ and $\angle S_{21}$, namely a "golden sample" that the AUT module is operated unimpaired. The subject of the training dataset is the attenuator and the phase shifter with the control codes {000000, 000001, 000010, 000100, 001000, 010000, 100000}. For each code, the target $|S_{21}|$ (denoted as $|S_{21}^T|$) and the target $\angle S_{21}$ (denoted as $\angle S_{21}^T$) are estimated by the mean of the measured data. In addition, the standard deviation estimate of $|S_{21}|$ and that of $\angle S_{21}$, denoted as $\hat{\sigma}_A$ and $\hat{\sigma}_P$, respectively, are computed by the sample standard deviation

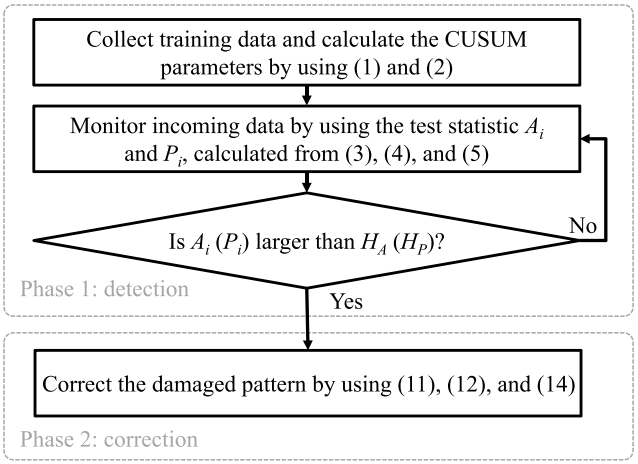

FIGURE 5. Flowchart of the proposed technique that integrates the detection of element failures and the correction of damaged patterns.

of the training data. In our experimental experience, a sample size of 10 observations is sufficient for the training dataset.

The proposed technique requires two parameters in the phase one:

$$K_A = \frac{|S_{21}^F| - |S_{21}^T|}{2}, \quad H_A = h_A \hat{\sigma}_A \text{ (dB)} \tag{1}$$

$$K_P = \frac{\angle S_{21}^F - \angle S_{21}^T}{2}, \quad H_P = h_P \hat{\sigma}_P \left(^\circ\right) \tag{2}$$

where K_A (K_P) and H_A (H_P) is the slack value and the decision threshold for the detection of the attenuator (phase shifter), respectively, $|S_{21}^F|(\angle S_{21}^F)$ is the expected measured value if the control code under test of the attenuator (phase shifter) is failed, and h_A (h_P) is the multiple of the standard deviation estimate. For example, when the attenuator with the code 000001 is tested, $K_A = 0.5$ dB / 2 $= 0.25$ dB because the failure of this code leads to a 0.5-dB difference. Another example is the phase shifter with the control code 000010. In this case, $K_P = 11.25^\circ / 2 = 5.625^\circ$, for 000010 is mapped to a phase shift of 11.25°. The selection of optimal h_A and h_P depends on the shift in the process mean that a user intends to detect [75]. In our application, as the element with a large failed code such as 100000 and 010000 is relatively easy to be found, we aim to select optimum h_A and h_P so that the failure of relatively small codes, especially 000001 and 000010, can be detected. In this case, setting the multiples to 4 or 5 generally provides a CUSUM having high sensitivity against a shift of about one standard deviation [76].

The incoming time-series data of $|S_{21}|$ and $\angle S_{21}$ are readily transformed to new test statistics A^i and P^i:

$$A^i = \max\left[0, \left|S_{21}^i\right| - \left(\left|S_{21}^T\right| + K_A\right) + A^{i-1}\right] \text{ (dB)} \tag{3}$$

$$P^i = \max\left[0, \angle S_{21}^i - \left(\angle S_{21}^T + K_P\right) + P^{i-1}\right] \left(^\circ\right) \tag{4}$$

where i denotes the i^{th} sample. To improve the sensitivity of fault finding, we incorporate a fast initial response (FIR) mechanism into the CUSUM process [77]. A 50% headstart

is employed to the initial value of A^i and P^i:

$$A^0 = \frac{H^A}{2}\,(\text{dB})\,, \quad P^0 = \frac{H^P}{2}\,(^\circ) \tag{5}$$

The sensitivity for detecting both small and large control codes can be thus enhanced.

In (3) and (4), A^i and P^i accumulates deviations from the target value that is greater than K_A and K_P, respectively. Thus, even though the smallest control code is defective, this small shift can be accumulated and become more significant. Finally, if $A^i(P^i)$ exceeds the decision interval H_A (H_P), the attenuator (phase shifter) with that code is evaluated as defective.

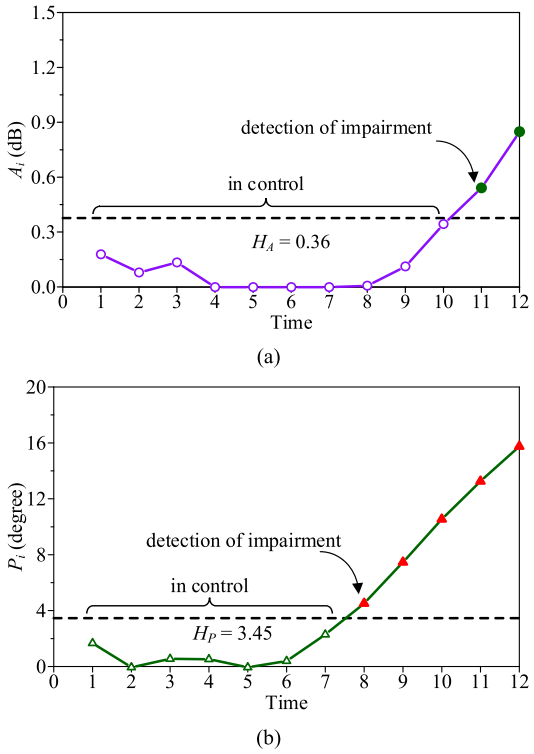

FIGURE 6. CUSUM control charts that monitor (a) the failure of an attenuator and (b) that of a phase shifter.

For example, Fig. 6 shows the graphical display of the CUSUM, which is constructed by plotting A^i or P^i in period i. In particular, Figs. 6 (a) and (b) represents the detection of the attenuator with the code 000001 and that of the phase shifter with the same code, respectively. The sample size of the training dataset is 10. $\hat{\sigma}_A$ and $\hat{\sigma}_P$ is 0.07 dB^2 and 0.69 square degrees, respectively. The CUSUM parameters are $K_A = 0.25, K_P = 2.8125, H_A = 0.36$, and $H_P = 3.45$. With the decision interval plotted on the chart, the user of the CUSUM can visualize that the 10$^{\text{th}}$ observation of the attenuator and the 8$^{\text{th}}$ observation of the phase shifter are out of control. This further indicates that the TR module is failed at that time period.

We program the above detection procedure via Visual Basic 6.0 with a graphical user interface (GUI). Fig. 7 presents the sample of a detection result for the 448-element active

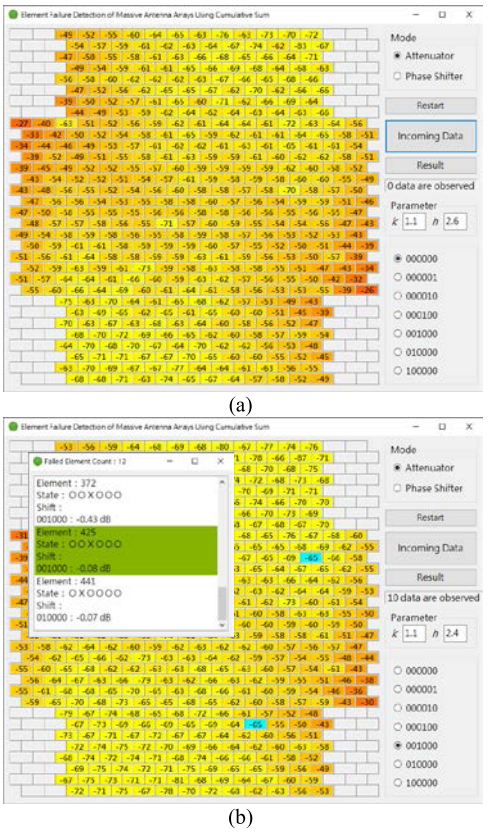

FIGURE 7. Graphical user interfaces of the proposed technique for (a) loading the incoming data and (b) showing the information on element failures.

phased array. The graphical appearance is according to the layout arrangement of the array elements. A user first loads the S_{21} of the training dataset, and our program automatically determines the CUSUM parameters. Next, the user loads the incoming S_{21} to be tested, and the program converts them to A^i and P^i, which indicate whether the TR module is defective by making a comparison with H_A and H_P. Such a GUI appearance facilitates the identification of the number and the locations of failed elements. The user can be aware of which TR module and which digital code are impaired by the blue grids shown in Fig. 7 (b). The performance of the failure detection will be presented in Section IV.

B. PHASE TWO: CORRECTION OF DAMAGED PATTERNS

Next, the proposed technique performs time series forecasting to determine the new excitations. The most distinct feature of the CUSUM chart is that it can provide an unbiased estimate of the new mean, which is what other SPC schemes such as the Shewhart control chart cannot offer. By using the test statistics of the CUSUM scheme, the new mean of the process is expressed as [76]:

$$\hat{\mu}_A = \left|S_{21}^T\right| + K_A + \frac{A^+}{N_A^+}\,(\text{dB}) \tag{6}$$

$$\hat{\mu}_P = \angle S_{21}^T + K_P + \frac{P^+}{N_P^+}\,(^\circ) \tag{7}$$

where $\hat{\mu}_A$ and $\hat{\mu}_P$ is the expected value of the new mean of the failed attenuator and that of the failed phase shifter, respectively, N_A^+ and N_P^+ is the counter that counts backward from the out-of-control signal to the time period when the CUSUM lifted above zero for $A^i$and P^i, respectively, and A^+ and P^+ are the associated value of that out-of-control signal. Let us consider the example shown in Fig. 6 (a). In period 11, $A^i$is evaluated as out of control, so $A^+ = 0.5426$ and $N_A^+ = 4$. According to (6), the new process mean is estimated as $\hat{\mu}_A = -57.73 + 0.25 + 0.5426/4 = -57.344$ dB. By such, the expected value of the new mean for all the faulty components can be computed.

These new means can be employed for compensating for the failed TR modules. Consider that the result of the phase one indicates that an array has m unimpaired elements and n defective elements. We express the element excitations $\mathbf{X}$ as a vector form:

$$\mathbf{X} = \left[\, \mathbf{X_U}\ \mathbf{X_F} \,\right]^T \text{(A)} \tag{8}$$

where $\mathbf{X_U}$ is the excitations of the m unimpaired elements and $\mathbf{X_F}$ is the excitations of the n defective elements. The elements of $\mathbf{X}$ are the polar form of complex numbers, whose magnitude and polar angle represents the current amplitude and phase, respectively.

The far-field vector-form radiation pattern $\mathbf{E}(\theta, \varphi)$ that results from these excitations can be expressed as:

$$\mathbf{E}\,(\theta, \phi) = \mathbf{H}\,(\theta, \phi)\,\mathbf{X}\,\text{(V)} \tag{9}$$

where $\mathbf{H}(\theta, \varphi)$ is the geometry dependent matrix, the element H_{ij} of which is:

$$H_{ij} = D_j\,(\theta_i, \phi_i)\, e^{jk[\sin\theta_i \cos\phi_i x_j + \sin\theta_i \cos\phi_i y_j + \cos\theta_i z_j]} \tag{10}$$

where $D_j(\theta_i, \varphi_i)$ is the directivity of the j^{th} element in the direction (θ_i, φ_i), k is the wave number, and x_j, y_j, and z_j are the coordinates of the position vectors of the j^{th} element.

The objective of the phase two is to determine $\mathbf{X}$ that leads to recovery as close as possible of the original pattern, denoted as $\mathbf{E_O}(\theta, \varphi)$. As the faulty elements and the associated expected value of the new mean have been obtained, the new excitations of the faulty elements are first multiplied by a compensation scalar. This operation results in a vector $\mathbf{X'}$:

$$\mathbf{X}' = \mathit{times}\,(\mathbf{C}, \mathbf{X})\,\text{(A)} \tag{11}$$

Here the operator $\mathit{times}(\mathbf{C}, \mathbf{X})$ represents element-wise multiplication of the two matrices$\mathbf{C}$ and $\mathbf{X}$, which have the same dimensions. The compensation scalars for the defective elements are computed by (6) and (7), and they are expressed as a vector form $\mathbf{C}$:

$$\mathbf{C} = \left[\, 1 \cdots 1\ \hat{\mu}_A \big/ |S_{21}^T| \cdots e^{jk\left(\hat{\mu}_P - \angle S_{21}^T\right)} \,\right]^T \tag{12}$$

The first m elements of $\mathbf{C}$ are unity, which are followed by n compensation scalars for those failed elements. In particular, for the failed attenuators, the excitations are calibrated by multiplying $\hat{\mu}_A/|S_{21}^T|$; on the other hand, for the failed phase shifters, the excitations are multiplied by $e^{jk\left(\hat{\mu}_P - \angle S_{21}^T\right)}$. Although the unit of $\hat{\mu}_A$ and that of $\hat{\mu}_P$ expressed in (6) and (7) is dB and degree, respectively, $\hat{\mu}_A$ in (12) is put in linear scale and the unit of $\hat{\mu}_P$ is put in radian.

To correct the damaged pattern, it is desired that $\mathbf{E'}(\theta, \varphi) = \mathbf{H}(\theta, \varphi)\ \mathbf{X'}$ is as close as possible to $\mathbf{E_O}(\theta, \varphi)$. This is equivalent to:

$$\min_{\mathbf{X}'} \left\| \mathbf{E_o} - \mathbf{E}' \right\| = \min_{\mathbf{X}'} \left\| \mathbf{E_o} - \mathbf{H}\mathbf{X}' \right\| \tag{13}$$

where $||\cdot||$ represents the norm of a vector. By using the least-squares estimate [78], the optimum solution of this problem is:

$$\hat{\mathbf{X}}' = \left(\mathbf{H}^T\mathbf{H}\right)^{-1}\mathbf{H}^T\mathbf{E_o}\,\text{(A)} \tag{14}$$

Thus, converting $\hat{X}$ to digital code subject to bypass the failed bits provides the excitations for TR modules. The advantage of the phase two is the high efficiency and simple in implementation. Our additional study suggests that integrating iterative weighted least-squares methods [79], [80] into the phase two can enhance the accuracy. However, with the above procedure, which performs only one iteration of computation, the performance is generally satisfactory and will be presented in Section V.

IV. PERFORMANCE OF DETECTION

In this section, we report the results of element failure detection using the CUSUM. To quantify the performance of fault finding, two performance indices should be evaluated, including a type I error and a type II error. The type I error means that a TR module is evaluated as faulty but in fact it is unimpaired. In other words, the type I error leads to a false alarm, which incurs additional costs if a user removes this unimpaired TR module. The type II error is that a detection algorithm does not sound an alarm but the TR module has been failed. Such a wrong decision degrades a radiation pattern. In general, every detection algorithm is challenged by both types of errors because the OTA test accompanies the fading with a stochastic nature; thus, a detection method should show the capability of minimizing them.

A. CONVENTIONAL MUTUAL COUPLING METHOD

First of all, we evaluate the performance of the conventional mutual coupling method. Fig. 8 presents the flowchart of the use of specification limits. This technique has been employed in the National Chung-Shan Institute of Science and Technology, a military organization in Taiwan. This detection method first collects a golden sample for every AUT, and the mean of $|S_{21}|$ and that of $\angle S_{21}$ are recorded for the control codes {000000, 000001, 000010, 000100, 001000, 010000, 100000} of each AUT. Next, a TA measures the $|S_{21}|$ of an AUT module at the zero state, namely 000000, to test whether the attenuator is failed. Once the measured $|S_{21}|$ is 6 dB lower than the corresponding value in the golden sample, the attenuator is evaluated as defective. Afterward,

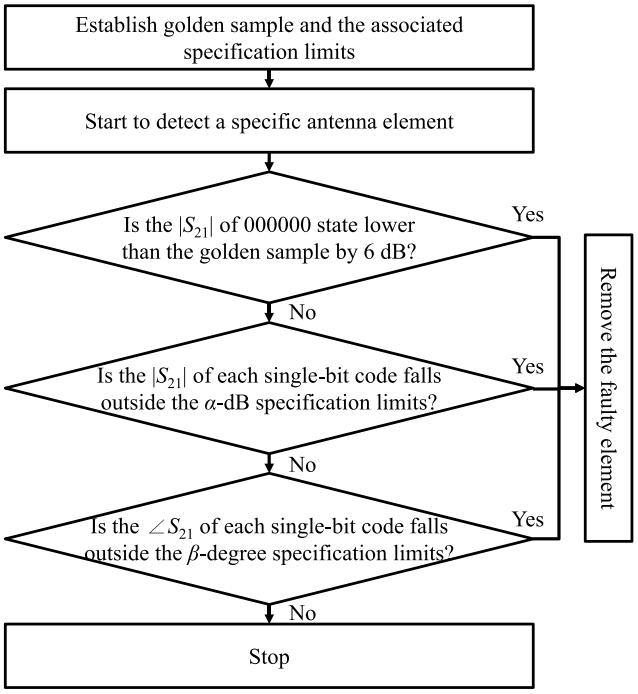

FIGURE 8. Flowchart of the conventional mutual coupling method using specification limits.

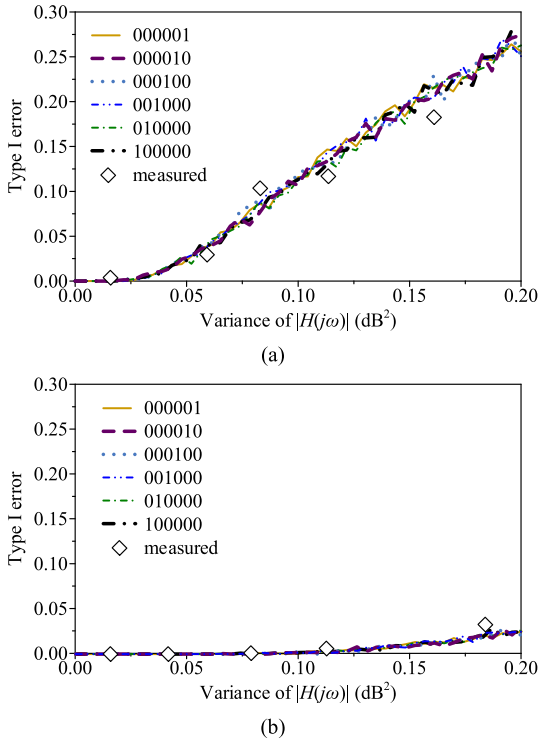

FIGURE 9. Simulated and measured type I errors of attenuators using the conventional mutual coupling method. (a) $\alpha = 0.5$. (b) $\alpha = 1$.

the attenuator with a single-bit code is tested. If the measured $|S_{21}|$ is α dB lower than the associated mean of the golden sample, this bit is evaluated as failed, where α is a parameter establishing the specification limits. Typically, setting $\alpha = 0.5$ is a straightforward choice because the attenuation step is 0.5 dB. Subsequently, this technique collects $\angle S_{21}$ for the phase shifter and tests all the single-bit codes. If the measured $\angle S_{21}$ is β degree lower than the mean angle of the golden sample, the phase shifter with this code is evaluated as failed. Likewise, β is a parameter and is usually selected as 5.625 following the unit phase step.

The type I and type II errors of the conventional technique are evaluated by performing simulation and measurement. The simulation is carried out by means of Monte Carlo experiments. To generate the mutual coupling data, we use Gamma distribution to emulate the fading that influences $|S_{21}|$. Gamma distribution is widely used in modeling the fading because it is mathematically sound and it can sufficiently approach the Lognormal distribution [81]. The probability density function is expressed as:

$$p_\gamma(\gamma) = \frac{\gamma^{s-1}}{\Gamma(s)\,\Omega^s} \exp\left(-\frac{\gamma}{\Omega}\right), \quad \gamma,\ \Omega,\ s \geq 0 \qquad (15)$$

where $\gamma$is the channel fade amplitude and s and Ω represents the shape and scale parameters of the Gamma distribution, respectively. The random variables of the amplitude of channel response, namely $|H(j\omega)|$, are generated according to (15). Meanwhile, the random variables of the phase of channel response, namely $\angle H(j\omega)$, are generated using a standard normal distribution with zero mean. For each variance considered, the generation of the random variables is repeated by 10^6 trials. These data are added to the attenuated value P_t and the level of phase shift φ_t for an AUT module, which finally provides the simulated S_{21} observations.

By such, we first construct the golden sample of S_{21} and the associated specification limits. Afterward, we consider that the attenuator under test is unimpaired and generate the incoming S_{21}. Fig. 9 (a) shows the simulated type I error for the six control codes. As expected, when the variance of the channel transfer function increases, the probability of false alarm is increased. This indicates that as the fading becomes serious, the probability for making a wrong decision is increased. All the control codes have an identical trend.

The simulated results are verified by measuring the 448-element active phased array. After a golden sample is collected, each unimpaired AUT module is tested for 10 samples, and the procedure repeats for every single-bit control code. We evaluate the incoming $|S_{21}|$ data by using the conventional method, computing the resultant type I error, shown in Fig. 9 (a). The simulated and measured results agree well. More explicitly, Table 2 summarizes the number of the type I error for each control code. As a relatively large attenuation is employed, such as 100000, the number of false alarms escalates. The underlying reason is examined by the estimate of the average variance of $|H(j\omega)|$. Fig. 10 represents the average variance of $|H(j\omega)|$ versus the magnitude of the mutual coupling of the 4,480 data collected. We calculate the average variance for each level of $|S_{21}|$. The result shows that a smaller $|S_{21}|$ leads to a low signal-to-noise ratio, and thus the variance of $|H(j\omega)|$ is relatively large. This situation

TABLE 2. The number of type I error for attenuators out of 4,480 tests.

Control code	Specification limit ($\alpha = 0.5$)	Specification limit ($\alpha = 1$)	CUSUM (proposed)
000000	0	0	0
000001	8	0	0
000010	22	1	0
000100	27	2	0
001000	34	3	0
010000	100	9	0
100000	768	219	0

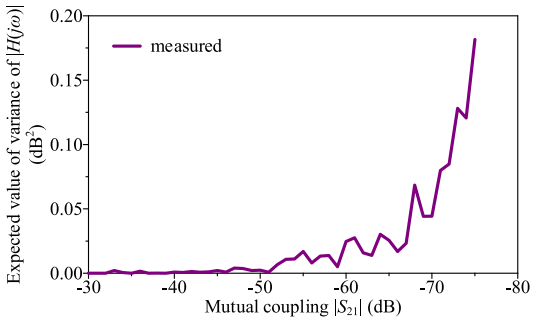

FIGURE 10. Variance of the measured data as the function of $|S_{21}|$.

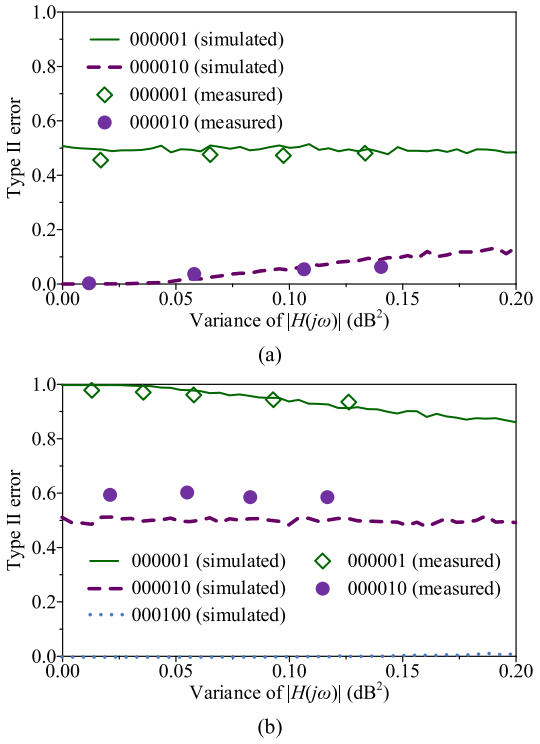

FIGURE 11. Simulated and measured type II errors of attenuators using the conventional mutual coupling method. (a) $\alpha = 0.5$. (b) $\alpha = 1$.

usually results from a large spacing between the AUT and the TA as well as a large control code.

A straightforward method to reduce the number of false alarms is to increase α as two attenuation steps, namely $\alpha = 1$. The associated simulated and measured results are shown in Fig. 9 (b) and Table 2. As the specification limits are relaxed, the number of false alarms can be reduced; however, this method incurs serious type II errors. The probability of the type II error is simulated for each single-bit control code. We generate the $|S_{21}|$ data that represent a failed attenuator, counting the number of data falling into the specification limits simply because of the fading. The simulated and measured results are shown in Fig. 11, and the detailed measured statistics are provided in Table 3. Whatever α is used, the relatively large control codes, including 000100, 001000, 010000, and 100000, show nearly zero type II error. This is not surprising because the failure of large attention values is inherently easier to be detected. However, the conventional method suffers from serious type II errors for the small control codes, including 000001 and 000010. When the specification limits are set to one attenuation step ($\alpha = 0.5$), 50% of draws with the code 000001 fall in the specification limits, but the attenuator has been set to the faulty state, namely 000000. Thus, 50% of failed attenuators with the code 000001 cannot be detected using the conventional method. Moreover, if the specification limits are set to two attenuation steps ($\alpha = 1$), the probability of the type II error for the 000001 state and the 000010 state becomes about 1 and 0.5, respectively. Thus, although increasing α reduces the type I error for the large control codes, this method cannot detect the failure of attenuators with the small control codes.

TABLE 3. The number of type II error for attenuators out of 4,480 tests.

Control code	Specification limit ($\alpha = 0.5$)	Specification limit ($\alpha = 1$)	CUSUM (proposed)
000001	2074	4376	100
000010	68	2813	19
000100	10	33	11
001000	0	0	0
010000	0	0	0
100000	0	0	0

Using this method, we also test the type I and type II errors of phase shifters. Fig. 12 shows the simulated and measured type I error. Detailed measured results are presented in Table 4. Our results show that the detection of phase shifters is independent of the variance of $\angle H(j\omega)$. The detection of phase information is relatively stable, and thus no type I error presents. However, there are severe type II errors for the phase shifters with the small control codes (000001 and 000010). Fig. 13 presents the simulated and measured results, and Table 5 summarizes the detailed measured observations out of 4,480 tests. When the phase shifter with the code 000001 fails, the conventional method with $\beta = 5.625$ incurs severe type II errors. As the distribution of $\angle S_{21}$ is symmetric and 50% of data fall in the specification limits,

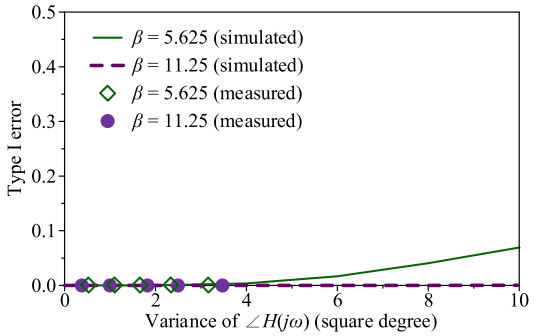

FIGURE 12. Simulated and measured type I errors of phase shifters using the conventional mutual coupling method.

TABLE 4. The number of type I error for phase shifters out of 4,480 tests

Control code	Specification limit ($\beta = 5.625$)	Specification limit ($\beta = 11.25$)	CUSUM (proposed)
000001	0	0	0
000010	0	0	0
000100	0	0	0
001000	0	0	0
010000	0	0	0
100000	0	0	0

the simulated probability of the type II error is as large as 50%. In addition, increasing β as two phase shift steps ($\beta = 11.25$) makes the detection process more difficult. In sum, the conventional detection method has two limitations: severe type I errors for the attenuator with the large control codes and serious type II errors for both attenuators and phase shifters with the small control codes.

B. CUSUM

These limitations can be overcome by using the CUSUM. We apply the proposed algorithm to the 448-element active phased array, establishing the training dataset and the associated parameters according to (1)–(5). Similarly, 10 incoming mutual coupling data are collected and tested. As a result, the number of the type I error for attenuators is provided in Table 2. No false alarms are found using the CUSUM. As compared to the conventional technique, this is a significant improvement that reduces the cost of unnecessary element replacement. The improvement is because the CUSUM takes the variation of the mutual coupling into account; as the alarm signaling is compared to the variance of $|S_{21}|$, the decision threshold for the attenuators with large control codes such as 100000 is adjusted adaptively. In addition, the number of the type I error for phase shifters is shown in Table 4, which also points out that the proposed method has no type I error.

The number of the type II error for the attenuators is shown in Table 3. While the conventional method fails to detect the impairment of the attenuators with the smallest control

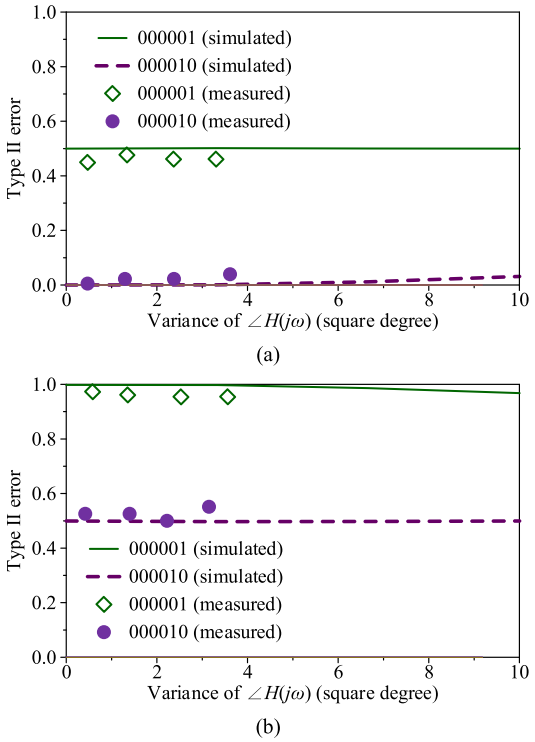

FIGURE 13. Simulated and measured type II errors of phase shifters using the conventional mutual coupling method. (a) $\beta = 5.625$. (b) $\beta = 11.25$.

TABLE 5. The number of type II error for phase shifters out of 4,480 tests

Control code	Specification limit ($\beta = 5.625$)	Specification limit ($\beta = 11.25$)	CUSUM (proposed)
000001	2008	4341	219
000010	129	2333	1
000100	0	0	0
001000	0	0	0
010000	0	0	0
100000	0	0	0

code, the CUSUM successfully achieves the fault finding. By cumulating the differences, the shift in the mean is thus detected even though the attenuation value is as small as 0.5 dB. Similarly, Table 5 presents the number of the type II error for the phase shifters. Once again, the proposed method successfully detects the failure of the phase shifters with the smallest control code.

More explicitly, the probability of successful detection for the attenuators and the phase shifters is shown and compared in Figs. 14 and 15, respectively. These figures point out that the accuracy of fault finding is significantly enhanced by using the CUSUM.

The sensitivity of the CUSUM can be quantified by the average run length (ARL). The ARL is defined as the number of test between a failure presented and an alarm. The smaller the ARL, the better the sensitivity is. The ARL can be evaluated as $1/\left[1 - \Pr(\text{typeIIerror})\right]$ [76]. According to Tables 3 and 5, the ARL of the detection for the attenuators

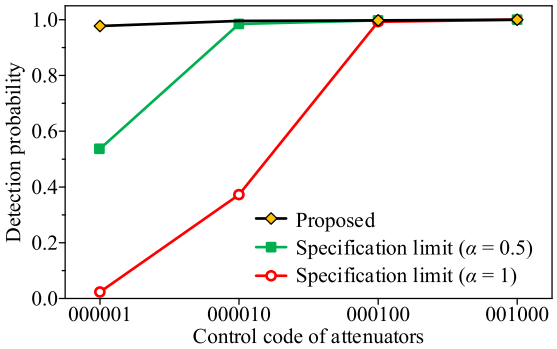

FIGURE 14. Comparison of detection probability for the failure of attenuators.

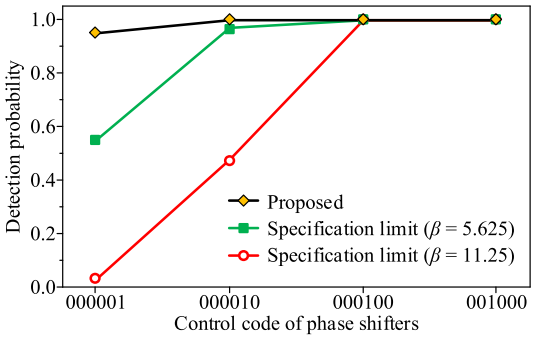

FIGURE 15. Comparison of detection probability for the failure of phase shifters.

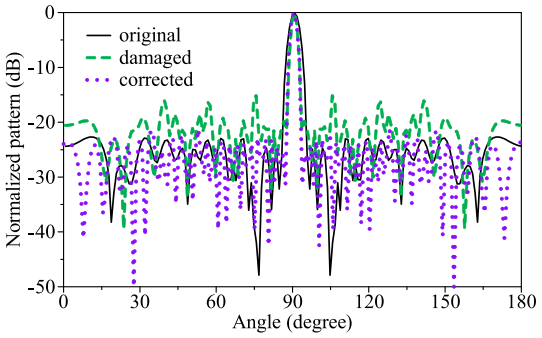

FIGURE 16. Radiation pattern of a 32-element linear active phased array with 10 failed attenuators and main beam pointing at broadside.

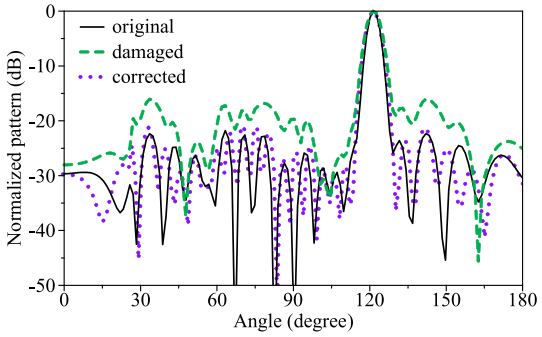

FIGURE 17. Radiation pattern of a 32-element linear active phased array with 5 failed attenuators and 5 failed phase shifters. The main beam points at 120°.

with the 000001 code and that for the phase shifters with the same code is 1.02 and 1.05, respectively, which means that the CUSUM can readily detect the fault of TR modules. As the FIR mechanism is incorporated by using a 50% head-start, the CUSUM achieves high sensitivity.

V. PERFORMANCE OF CORRECTION

The phase two of the proposed technique is demonstrated via three examples. The first and second examples are a linear array with 32 identical printed dipoles having uniform half wavelength spacing between adjacent elements. These dipoles are placed along the x-axis, and the center of the array corresponds to the origin. The first example uses Dolph-Chebyshev excitations with a SLL of –25 dB and a main beam at broadside. There are 10 defective elements considered, located symmetrically at the first, fifth, ninth, sixteenth, seventeenth, twenty-fourth, twenty-eighth, and thirty-second position, respectively; each element has a failed bit in their attenuator, but the phase shifter is unimpaired. Thus, the imperative of both central and edge elements is represented. The failed bits are intentionally set to the 0 state. We apply the phase one of the proposed technique to detect these element faults. Afterward, the phase two is employed to calculate the new excitations, but the impaired bits remain the 0 state.

Fig. 16 depicts the original radiation pattern without element failures. The maximum SLL is –23.5 dB. This level is slightly different to the desired one because of a digitalization error. When the components at the above-mentioned locations become defective, the maximum SLL increases to –15.1 dB at 75.8°, as shown in the same figure. By performing the phase two of the proposed technique, the corrected pattern, also shown in Fig. 16, recovers the SLL while retaining a broadside radiation. The maximum SLL is improved from –15.1 dB to –21.9 dB. Considering that the digitalization error is represented and only one iteration of computation is required, the performance of pattern recovery is satisfactory.

The second example also uses Dolph-Chebyshev excitations with an SLL of –25 dB, but the main beam points at 120°. In this case, 10 defective elements including 5 attenuators and 5 phase shifters are considered. The failed attenuators is located at the third, ninth, tenth, seventeenth, and twenty-fifth position, respectively, and the failed phase shifters is located at the first, fourteenth, sixteenth, twenty-seventh, and thirty-second position, respectively, all with a one-bit failure.

Fig. 17 shows the original pattern without element failures, the damaged pattern that results from the above-mentioned condition, and the corrected pattern by using the proposed technique. The main beams of the three cases point to the same direction, as the failure of the phase shifters does not significantly change the arrangement of a progressive phase. However, the maximum SLL of the damaged pattern decreases from –22.1 dB to –15.3 dB at 34.9°. The degradation of the pattern is successfully recovered using the proposed technique. The maximum SLL becomes –21.9 dB, which is close to the original level.

The third example is a planar array with 8×8 elements having identical half wavelength spacing between adjacent elements. These elements are placed on the x-y plane, and

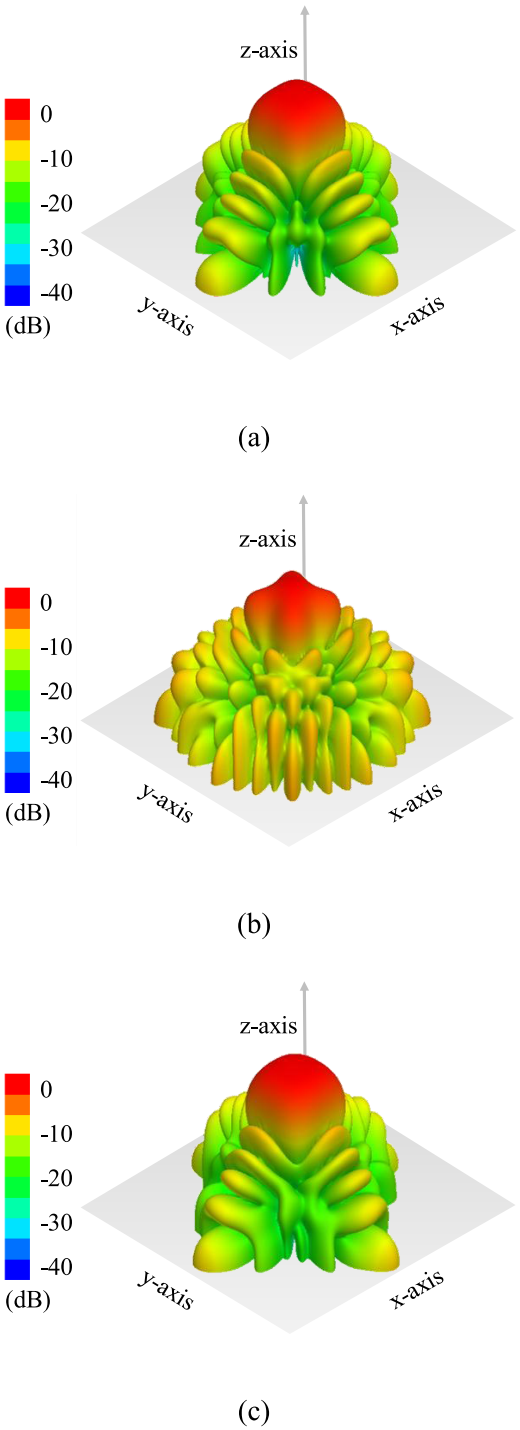

FIGURE 18. Flat-top radiation pattern of a 64-element planar active phased array with 10 failed attenuators and 10 failed phase shifters. (a) Original. (b) Damaged. (c) Corrected.

the center of the array corresponds to the origin. The current excitations of this array are to have a flat-top main beam pointing at broadside. There are 10 failed attenuators and 10 phase shifters in this array. The locations of the failed components and the associated defective bits are arbitrarily assigned.

Following the same methodology, the original pattern, the damaged pattern, and the corrected pattern is shown in Figs. 18 (a), (b), and (c), respectively. The half-power beam width (HPBW) of the original pattern is 28° on the x-z plane and 28° on the y-z plane. When the 20 elements are impaired, the HPBW becomes 17° on the x-z plane and 15° on the y-z plane. The main beam of the damaged pattern has concaves at some directions, and thus this result does not meet the requirement of a flat-top pattern. When the pattern is corrected using the proposed method, the HPBW is 27° on the x-z plane and 26° on the y-z plane. Accordingly, the HPBWs are successfully recovered.

In addition to the capability of correcting damaged patterns, the proposed technique shows high efficiency as compared to the correction using heuristic algorithms [48]–[65]. As the proposed method does not treat the problem as a black box, using the data that result from the phase one reduces the computational times in the phase two. On the other hand, although the proposed technique can correct a damaged pattern with a similar main beam characteristic and a desired SLL, the direction of nulls cannot be fully recovered. There have been studies in the literature dealing with the recovery of null steering by a pattern correction algorithm [54], [65]. We will integrate a null steering technique into the phase two in our future work.

VI. CONCLUSION

We have presented a novel technique based on the CUSUM for the detection of array element failures and the correction of damaged radiation patterns. The significance of this work is threefold. First, while the literature treats the detection and the correction as related issues but separated procedures, our proposed method organizes the two subjects into a systematic process. By using the data from the detection phase, the correction phase can recover a damaged pattern through the least-squares estimation. Moreover, this systematic procedure is simple in implementation, requiring neither blind search nor iterative computation.

Second, the detection phase overcomes the limitation of the conventional mutual coupling method, which incurs severe type I and type II errors in the detection of the large and small control codes, respectively. The effectiveness of the proposed technique has been validated through a 448-element array. The number of both types of errors is significantly reduced, and the detection sensitivity is satisfactory.

Third, the correction phase shows high accuracy with reduced computational complexity. The capability of the pattern correction has been demonstrated via three examples when as many as 30% of the elements are defective. In all the scenarios, the proposed method is capable of suppressing SLLs and preserving the characteristic of main beam. Given its attractive features and satisfactory performance, the proposed CUSUM scheme is particularly suitable to be implemented in the active phased arrays using a mutual coupling calibration.

REFERENCES

[1] E. Björnson, M. Matthaiou, and M. Debbah, "Massive MIMO with non-ideal arbitrary arrays: Hardware scaling laws and circuit-aware design," *IEEE Trans. Wireless Commun.*, vol. 14, no. 5, pp. 4353–4368, Aug. 2014.

[2] L. A. Rondinelli, "Effects of random errors on the performance of antenna arrays of many elements," in *Proc. IRE Int. Conv. Rec.*, 1959, pp. 174–189.
[3] X. Li, L. Li, L. Xie, X. Su, and P. Zhang, "Performance analysis of 3D massive MIMO cellular systems with collaborative base station," *Int. J. Antennas Propag.*, vol. 2014, Jul. 2014, Art. no. 614061.
[4] M. Karman, H. Köymen, A. Atalar, and M. O'Donnell, "Influence of missing array elements on phase aberration correction for medical ultrasound," *IEEE Trans. Ultrason., Ferroelect., Freq. Control*, vol. 41, no. 5, pp. 613–620, Sep. 1994.
[5] J. A. Rodriguez-Gonzalez, F. Ares-Pena, M. Fernandez-Delgado, R. Iglesias, and S. Barro, "Rapid method for finding faulty elements in antenna arrays using far field pattern samples," *IEEE Trans. Antennas Propag.*, vol. 57, no. 6, pp. 1679–1683, Jun. 2009.
[6] O. M. Bucci, A. Capozzoli, and G. D'Elia, "Diagnosis of array faults from far-field amplitude-only data," *IEEE Trans. Antennas Propag.*, vol. 48, no. 5, pp. 647–652, May 2000.
[7] P. Mukherjee, B. Gupta, and K. Yasumoto, "Element failure detection in linear antenna arrays using case-based reasoning," in *Proc. Int. Symp. Antennas Propag.*, Niigata, Japan, Aug. 2007, pp. 330–333.
[8] R. Iglesias, F. Ares, M. Fernandez-Delgado, J. A. Rodriguez, J. Bregains, and S. Barro, "Element failure detection in linear antenna arrays using case-based reasoning," *IEEE Antennas Propag. Mag.*, vol. 50, no. 4, pp. 198–204, Aug. 2008.
[9] J. A. Rodríguez and F. Ares, "Finding defective elements in planar arrays using genetic algorithms," *Prog. Electromagn. Res.*, vol. 29, pp. 25–37, 2000.
[10] A. Patnaik, B. Choudhury, P. Pradhan, R. K. Mishra, and C. Christodoulou, "An ANN application for fault finding in antenna arrays," *IEEE Trans. Antennas Propag.*, vol. 55, no. 3, pp. 775–777, Mar. 2007.
[11] G. Castaldi, V. Pierro, and I. M. Pinto, "Efficient faulty element diagnostics of large antenna arrays by discrete mean field neural nets," *Prog. Electromagn. Res.*, vol. 25, pp. 53–76, 2000.
[12] D. Vakula and N. V. S. N. Sarma, "Fault diagnosis of planar antenna arrays using neural networks," *Prog. Electromagn. Res. M*, vol. 6, pp. 35–46, 2009.
[13] D. Vakula and N. V. S. N. Sarma, "A method for diagnosis of current faults in antenna arrays using neural networks," *Int. J. RF Microw. Comput.-Aided Eng.*, vol. 19, no. 2, pp. 270–276, Mar. 2009.
[14] G. Oliveri, P. Rocca, and A. Massa, "Reliable diagnosis of large linear arrays—A Bayesian compressive sensing approach," *IEEE Trans. Antennas Propag.*, vol. 60, no. 10, pp. 4627–4636, Oct. 2012.
[15] M. D. Migliore, "A compressed sensing approach for array diagnosis from a small set of near-field measurements," *IEEE Trans. Antennas Propag.*, vol. 59, no. 6, pp. 2127–2133, Jun. 2011.
[16] K. C. S. Kavya *et al.*, "Array diagnosis using compressed sensing in near field," *J. Inf. Eng. Appl.*, vol. 2, no. 7, pp. 1–6, 2012.
[17] J. Park, J. Lee, J. Chun, and S. Kwak, "Robust monopulse beam synthesis with sparse elements in linear and planar arrays with element failure detection," *IET Radar Sonar Navig.*, vol. 11, no. 8, pp. 1251–1258, Aug. 2017.
[18] J. J. Lee, E. M. Ferren, D. P. Woollen, and K. M. Lee, "Near-field probe used as a diagnostic tool to locate defective elements in an array antenna," *IEEE Trans. Antennas Propag.*, vol. 36, no. 6, pp. 884–889, Jun. 1988.
[19] O. M. Bucci, M. D. Migliore, G. Panariello, and P. Sgambato, "Accurate diagnosis of conformal arrays from near-field data using the matrix method," *IEEE Trans. Antennas Propag.*, vol. 53, no. 3, pp. 1114–1120, Mar. 2005.
[20] M. D. Migliore, "Array diagnosis from far-field data using the theory of random partial Fourier matrices," *IEEE Antennas Wireless Propag. Lett.*, vol. 12, pp. 745–748, 2013.
[21] M. Carlin, G. Oliveri, and A. Massa, "On the robustness to element failures of linear ADS-thinned arrays," *IEEE Trans. Antennas Propag.*, vol. 59, no. 12, pp. 4849–4853, Dec. 2011.
[22] A. Buonanno and M. D'Urso, "On the diagnosis of arbitrary geometry fully active arrays," in *Proc. Eur. Conf. Antennas Propag.*, Barcelona, Spain, Apr. 2010, pp. 1–4.
[23] B. Choudhury, O. P. Acharya, and A. Patnaik, "Bacteria foraging optimization in antenna engineering: An application to array fault finding," *Int. J. RF Microw. Comput.-Aided Eng.*, vol. 23, no. 2, pp. 141–148, May 2012.
[24] H. M. Aumann, A. J. Fenn, and F. G. Willwerth, "Phased array antenna calibration and pattern prediction using mutual coupling measurements," *IEEE Trans. Antennas Propag.*, vol. 37, no. 7, pp. 844–850, Jul. 1989.
[25] Y. Neidman, R. Shavit, and A. Bronshtein, "Diagnostic of phased arrays with faulty elements using the mutual coupling method," *IET Microw., Antennas Propag.*, vol. 3, no. 2, pp. 235–241, Mar. 2009.
[26] S. H. Son, S. I. Jeon, and W. Hwang, "Automatic calibration method for phased arrays with arbitrary aperture shape," *Microw. Opt. Technol. Lett.*, vol. 50, no. 6, pp. 1590–1592, Jun. 2008.
[27] A. Agrawal and A. Jablon, "A calibration technique for active phased array antennas," in *Proc. IEEE Int. Symp. Phased Array Syst. Technol.*, Boston, MA, Oct. 2003, pp. 223–228.
[28] K. M. Webb, "Method and apparatus for phased array antenna field recalibration," U.S. Patent 8 154 452, Apr. 10, 2012.
[29] D. L. Collinson, "Mutual coupling method for calibrating a phased array," U.S. Patent 7 362 266, Apr. 22, 2008.
[30] C. Shipley and D. Woods, "Mutual coupling-based calibration of phased array antennas," in *Proc. IEEE Int. Conf. ARRAY*, Dana Point, CA, USA, May 2000, pp. 529–532.
[31] F. S. Gerino and P. M. Belcaguy, "Mutual coupling internal calibration method applied to a polarimetric phased array antenna model," in *Proc. Global Electromagn. Compat. Conf.*, Mar del Plata, Argentina, Nov. 2016, pp. 1–5.
[32] J. Vieira, F. Rusek, and F. Tufvesson, "A receive/transmit calibration technique based on mutual coupling for massive MIMO base stations," in *Proc. IEEE 27th Annu. Int. Symp. Pers., Indoor, Mobile Radio Commun.*, Valencia, Spain, Sep. 2016, pp. 1–6.
[33] R. Rotman, Y. Oz, and A. Benaish, "Calibration of large phased arrays including monopulse ratios," in *Proc. IEEE Antennas Propag. Soc. Int. Symp.*, Boston, MA, USA, Jul. 2001, pp. 622–625.
[34] D. Bekers, R. van Dijk, and F. van Vliet, "Mutual-coupling based phased-array calibration: A robust and versatile approach," in *Proc. IEEE Int. Symp. Phased Array Syst. Technol.*, Waltham, MA, USA, Oct. 2013, pp. 630–637.
[35] B. Chen, J. Ouyang, G. Wu, and R. Long, "A novel on-board and amplitude-only measurement method for phase array calibration," in *Proc. IEEE 5th Asia–Pacific Conf. Antennas Propag.*, Kaohsiung, Taiwan, Jul. 2016, pp. 221–222.
[36] T. Takahashi, Y. Konishi, S. Makino, H. Ohmine, and H. Nakaguro, "Fast measurement technique for phased array calibration," *IEEE Trans. Antennas Propag.*, vol. 56, no. 7, pp. 1888–1899, Jul. 2008.
[37] R. Yonezawa, Y. Konishi, I. Chiba, and T. Katagi, "Beam-shape correction in deployable phased arrays," *IEEE Trans. Antennas Propag.*, vol. 47, no. 3, pp. 482–486, Mar. 1999.
[38] R. Ishii, K. Shiramatsu, T. Haruyama, N. Orime, and T. Katagi, "A built-in correction method of the phase distribution of a phased array antenna," in *IEEE AP-S Int. Symp. Dig.*, London, ON, Canada, Jun. 1991, pp. 1144–1147.
[39] H.-T. Chou and D.-Y. Cheng, "Beam-pattern calibration in a realistic system of phased-array antennas via the implementation of a genetic algorithm with a measurement system," *IEEE Trans. Antennas Propag.*, vol. 65, no. 2, pp. 593–601, Feb. 2017.
[40] T. Takahashi *et al.*, "On-board calibration methods for mechanical distortions of satellite phased array antennas," *IEEE Trans. Antennas Propag.*, vol. 60, no. 3, pp. 1362–1372, Mar. 2012.
[41] M. D. Migliore, D. Pinchera, M. Lucido, F. Schettino, and G. Panariello, "A sparse recovery approach for pattern correction of active arrays in presence of element failures," *IEEE Antennas Wireless Propag. Lett.*, vol. 14, pp. 1027–1030, 2015.
[42] H. Pawlak and A. F. Jacob, "An external calibration scheme for DBF antenna arrays," *IEEE Trans. Antennas Propag.*, vol. 58, no. 1, pp. 59–67, Jan. 2010.
[43] K.-M. Lee, R.-S. Chu, and S.-C. Liu, "A built-in performance-monitoring/fault isolation and correction (PM/FIC) system for active phased-array antennas," *IEEE Trans. Antennas Propag.*, vol. 41, no. 11, pp. 1530–1540, Nov. 1993.
[44] S. Andersson, U. Forssén, F. B. Ovesjö, and S. O. Petersson, "Antenna array calibration," U.S. Patent 6 339 399, Jan. 15, 2002.
[45] E. Lee and C. N. Dorny, "A broadcast reference technique for self-calibrating of large antenna phased arrays," *IEEE Trans. Antennas Propag.*, vol. 37, no. 8, pp. 1003–1010, Aug. 1989.
[46] R. Sorace, "Phased array calibration," *IEEE Trans. Antennas Propag.*, vol. 49, no. 4, pp. 517–525, Apr. 2001.
[47] C. N. Hu, "A novel method for calibrating deployed active antenna arrays," *IEEE Trans. Antennas Propag.*, vol. 63, no. 4, pp. 1650–1657, Apr. 2015.
[48] B.-K. Yeo and Y. Lu, "Array failure correction with a genetic algorithm," *IEEE Trans. Antennas Propag.*, vol. 47, no. 5, pp. 823–828, May 1999.
[49] J. A. Rodriguez, F. Ares, E. Moreno, and G. Franceschetti, "Genetic algorithm procedure for linear array failure correction," *Electron. Lett.*, vol. 36, no. 3, pp. 196–198, Feb. 2000.

[50] S. A. Mitilineos, S. C. A. Thomopoulos, and C. N. Capsalis, "On array failure mitigation with respect to probability of failure, using constant excitation coefficients and a genetic algorithm," *IEEE Antennas Wireless Propag. Lett.*, vol. 5, no. 1, pp. 187–190, Dec. 2006.

[51] S. A. Mitilineos, S. C. A. Thomopoulos, and C. N. Capsalis, "Genetic design of dual-band, switched-beam dipole arrays, with elements failure correction, retaining constant excitation coefficients," *J. Electromagn. Waves Appl.*, vol. 20, no. 14, pp. 1925–1942, 2006.

[52] J.-H. Han, S.-H. Lim, and N.-H. Myung, "Array antenna TRM failure compensation using adaptively weighted beam pattern mask based on genetic algorithm," *IEEE Antennas Wireless Propag. Lett.*, vol. 11, pp. 18–21, 2012.

[53] J. A. Rodríguez and F. Ares, "Optimization of the performance of arrays with failed elements using the simulated annealing technique," *J. Electromagn. Waves Appl.*, vol. 12, no. 12, pp. 1625–1638, 1998.

[54] M. V. Lozano, J. A. Rodríguez, and F. Ares, "Recalculating linear array antennas to compensate for failed elements while maintaining fixed nulls," *J. Electromagn. Waves Appl.*, vol. 13, no. 3, pp. 397–412, 1999.

[55] O. P. Acharya, A. Patnaik, and S. N. Sinha, "Limits of compensation in a failed antenna array," *Int. J. RF Microw. Comput.-Aided Eng.*, vol. 24, no. 6, pp. 635–645, 2014.

[56] R. Muralidharan, A. Vallavaraj, G. K. Mahanti, and H. Patidar, "QPSO for failure correction of linear array of mutually coupled parallel dipole antennas with desired side lobe level and return loss," *J. King Saud Univ.-Eng. Sci.*, vol. 29, no. 2, pp. 112–117, 2017.

[57] Y. Yang and H. Stark, "Design of self-healing arrays using vector-space projections," *IEEE Trans. Antennas Propag.*, vol. 49, no. 4, pp. 526–534, Apr. 2001.

[58] K. Guney, A. Durmus, and S. Basbug, "Antenna array synthesis and failure correction using differential search algorithm," *Int. J. Antennas Propag.*, vol. 2014, 2014, Art. no. 276754.

[59] S. U. Khan, I. M. Qureshi, F. Zaman, A. Naveed, B. Shoaib, and A. Basit, "Correction of faulty sensors in phased array radars using symmetrical sensor failure technique and cultural algorithm with differential evolution," *Sci. World J.*, vol. 2014, 2014, Art. no. 852539.

[60] N. S. Grewal, M. Rattan, and M. S. Patterh, "A linear antenna array failure correction using firefly algorithm," *Prog. Electromagn. Res. M*, vol. 27, pp. 241–254, 2012.

[61] N. S. Grewal, M. Rattan, and M. S. Patterh, "A linear antenna array failure correction using improved bat algorithm," *Int. J. RF Microw. Comput.-Aided Eng.*, vol. 27, no. 7, p. e21119, Sep. 2017.

[62] S. Biswas, P. P. Sarkar, and B. Gupta, "Array factor correction using artificial neural network model," *Int. J. Electron.*, vol. 91, no. 5, pp. 301–308, May 2004.

[63] T. J. Peters, "A conjugate gradient-based algorithm to minimize the sidelobe level of planar arrays with element failures," *IEEE Trans. Antennas Propag.*, vol. 39, no. 10, pp. 1497–1504, Oct. 1991.

[64] M. H. Er and S. K. Hui, "Beamforming in presence of element failure," *Electron. Lett.*, vol. 27, no. 3, pp. 273–275, Jan. 1991.

[65] M. J. Mismar and T. H. Ismail, "Null steering with element failures using partial controlled linear arrays," *Electromagnetics*, vol. 23, no. 5, pp. 445–454, 2003.

[66] R. Janaswamy, D. V. Gupta, and D. H. Schaubert, "Adaptive correction to array coefficients through dithering and near-field sensing," *IEEE Trans. Antennas Propag.*, vol. 58, no. 11, pp. 3558–3567, Nov. 2010.

[67] R. J. Mailloux, "Array failure correction with a digitally beamformed array," *IEEE Trans. Antennas Propag.*, vol. 44, no. 12, pp. 1543–1550, Dec. 1996.

[68] W. P. M. N. Keizer, "Element failure correction for a large monopulse phased array antenna with active amplitude weighting," *IEEE Trans. Antennas Propag.*, vol. 55, no. 8, pp. 2211–2218, Aug. 2007.

[69] S. U. Khan, I. M. Qureshi, B. Shoaib, and A. Naveed, "Recovery of failed element signal with a digitally beamforming using linear symmetrical array antenna," *J. Inf. Sci. Eng.*, vol. 32, no. 3, pp. 611–624, 2016.

[70] G. Oliveri, M. Donelli, and A. Massa, "Linear array thinning exploiting almost difference sets," *IEEE Trans. Antennas Propag.*, vol. 57, no. 12, pp. 3800–3812, Dec. 2009.

[71] L. Lei, G. Zhang, and R. J. Doviak, "Bias correction for polarimetric phased-array radar with idealized aperture and patch antenna elements," *IEEE Trans. Geosci. Remote Sens.*, vol. 51, no. 1, pp. 473–486, Jan. 2011.

[72] M. Levitas, D. A. Horton, and T. C. Cheston, "Practical failure compensation in active phased arrays," *IEEE Trans. Antennas Propag.*, vol. 47, no. 3, pp. 524–535, Mar. 1999.

[73] J. L. Salazar, R. H. Medina, and E. Loew, "T/R modules for active phased array radars," in *Proc. IEEE Int. Radar Conf.*, Arlington, VA, USA, May 2015, pp. 1125–1133.

[74] D. C. Montgomery and G. C. Runger, *Applied Statistics and Probability for Engineers*. New York, NY, USA: Wiley, 2003, pp. 595–648.

[75] P. A. Rogerson, "Formulas for the design of CUSUM quality control charts," *Commun. Statist.-Theory Methods*, vol. 35, no. 2, pp. 373–383, Aug. 2006.

[76] D. C. Montgomery, *Introduction to Statistical Quality Control*. New York, NY, USA: Wiley, 2009, p. 406.

[77] J. M. Lucas and R. B. Crosier, "Fast initial response for CUSUM quality-control schemes: Give your CUSUM a head start," *Technometrics*, vol. 24, no. 3, pp. 199–205, Aug. 1982.

[78] P. N. Fletcher and M. Dean, "Least squares pattern synthesis for conformal arrays," *Electron. Lett.*, vol. 34, no. 25, pp. 2363–2365, Dec. 1998.

[79] L. I. Vaskelainen, "Iterative least-squares synthesis methods for conformal array antennas with optimized polarization and frequency properties," *IEEE Trans. Antennas Propag.*, vol. 45, no. 7, pp. 1179–1185, Jul. 1997.

[80] B. D. Carlson and D. Willner, "Antenna pattern synthesis using weighted least squares," *IEE Proc. H-Microw., Antennas Propag.*, vol. 139, no. 1, pp. 11–16, Feb. 1992.

[81] M. K. Simon and M.-S. Alouini, *Digital Communication over Fading Channels*. New York, NY, USA: Wiley, 2005, pp. 18–26.

YEN-SHENG CHEN (M'13) was born in Taichung, Taiwan, in 1985. He received the B.S. degree in electrical engineering and the M.S. and Ph.D. degrees in communication engineering from National Taiwan University, Taipei, Taiwan, in 2007, 2009, and 2012, respectively.

Since 2013, he has been a Faculty Member with the Department of Electronic Engineering, National Taipei University of Technology, Taipei, where he is currently an Associate Professor. He has participated in a wide range of research projects, including wireless power transfer, antenna array failure correction, antennas for body centric communications, multiple-input multiple-output antennas for compact base stations, microwave reconfigurable devices, and multi-objective optimization techniques. His recent research focus includes RF energy harvesting, antenna arrays, radio-frequency identification, and engineering data analysis/mining. He has served on the editorial/review boards of many technical journals, transactions, proceedings, and letters. He received an Outstanding Reviewer Award from the IEEE Antennas and Wireless Propagation Letters in 2017.

I-LIN TSAI was born in Tainan, Taiwan, in 1994. He received the B.S. degree in electronic engineering from the National Taipei University of Technology, Taipei, Taiwan, in 2017. He is currently pursuing the M.S. degree in electrical engineering with the National Taiwan University of Science and Technology, Taipei.

His current research interests include the design and analysis of self-oscillating active integrated antennas, intelligent transportation systems, and information engineering.